ITUPublications

International Telecommunication Union
Radiocommunication Sector

Report ITU-R M.2305-1

(11/2025)

M Series: Mobile, radiodetermination, amateur and related satellite services

Consideration of aggregate radio frequency interference event potentials from multiple Earth exploration-satellite service systems on radionavigation-satellite service receivers operating in the frequency band 1 215-1 300 MHz

Foreword

The role of the Radiocommunication Sector is to ensure the rational, equitable, efficient and economical use of the radio-frequency spectrum by all radiocommunication services, including satellite services, and carry out studies without limit of frequency range on the basis of which Recommendations are adopted.

The regulatory and policy functions of the Radiocommunication Sector are performed by World and Regional Radiocommunication Conferences and Radiocommunication Assemblies supported by Study Groups.

Policy on Intellectual Property Right (IPR)

ITU-R policy on IPR is described in the Common Patent Policy for ITU-T/ITU-R/ISO/IEC referenced in Resolution ITU-R 1. Forms to be used for the submission of patent statements and licensing declarations by patent holders are available from https://www.itu.int/ITU-R/go/patents/en where the Guidelines for Implementation of the Common Patent Policy for ITU-T/ITU-R/ISO/IEC and the ITU-R patent information database can also be found.

Series of ITU-R Reports

(Also available online at https://www.itu.int/publ/R-REP/en)

Series	Title
BO	Satellite delivery
BR	Recording for production, archival and play-out; film for television
BS	Broadcasting service (sound)
BT	Broadcasting service (television)
F	Fixed service
M	**Mobile, radiodetermination, amateur and related satellite services**
P	Radio-wave propagation
RA	Radio astronomy
RS	Remote sensing systems
S	Fixed-satellite service
SA	Space applications and meteorology
SF	Frequency sharing and coordination between fixed-satellite and fixed service systems
SM	Spectrum management
TF	Time signals and frequency standards emissions

***Note**: This ITU-R Report was approved in English by the Study Group under the procedure detailed in Resolution ITU-R 1.*

Electronic Publication
Geneva, 2026

REPORT ITU-R M.2305-1

Consideration of aggregate radio frequency interference event potentials from multiple Earth exploration-satellite service systems on radionavigation-satellite service receivers operating in the frequency band 1 215-1 300 MHz

(2014-2025)

TABLE OF CONTENTS

1 Introduction

The frequency band 1 215-1 300 MHz is allocated on a primary basis to the radiolocation service and radionavigation-satellite service (RNSS). This band is also allocated on a primary basis to the Earth exploration-satellite service (EESS) (active) for spaceborne active microwave sensors subject to the limitations of Radio Regulations Nos. **5.332** and **5.335A**. The ITU-R has developed a number of Reports and Recommendations useful for compatibility studies between EESS (active) and RNSS. In particular,

– Recommendation ITU-R M.1902 – Characteristics and protection criteria for receiving earth stations in the radionavigation-satellite service (space-to-Earth) operating in the band 1 215-1 300 MHz, specifies the characteristics and protection criteria for receiving earth stations in the RNSS operating in the frequency band 1 215-1 300 MHz. The continuous radio frequency interference (RFI) protection criteria in this Recommendation do not apply to pulsed RFI sources such as those used by EESS (active) sensors. However, certain RNSS receiver characteristics in Recommendation ITU-R M.1902 are useful for this Report.

– Recommendation ITU-R M.2030 – Evaluation method for pulsed interference from relevant radio sources other than in the radionavigation-satellite service to the radionavigation-satellite service systems and networks operating in the frequency bands 1 164-1 215 MHz, 1 215-1 300 MHz and 1 559-1 610 MHz, provides guidance on how to assess the impact of pulsed RFI sources on RNSS receivers.

– Report ITU-R M.2220 – Calculation method to determine aggregate interference parameters of pulsed RF systems operating in and near the bands 1 164-1 215 MHz and 1 215-1 300 MHz that may impact radionavigation-satellite service airborne and ground-based receivers operating in those frequency bands, provides a method and example on how to calculate the aggregate RFI parameters used in Recommendation ITU-R M.2030.

When signals from multiple pulsed RFI sources simultaneously illuminate RNSS receivers, the degradation equations in Recommendation ITU-R M.2030, along with the companion Report ITU-R M.2220, provide an approach to computation of the aggregate pulsed RFI impact. However, the determination of impingement statistics associated with these aggregate RFI events, i.e., how often, and for how long they occur, requires extensive satellite simulations.

The purpose of this Report is to provide results of a simultaneous illumination impingement study focusing on two EESS (active) systems. The organization of this Report is as follows: A brief description of pulsed RFI effects on RNSS receivers operating in the frequency band 1 215-1 300 MHz is provided in § 2. The EESS (active) sensors planned for deployment in the 1 215-1 300 MHz band are described in § 3. The analysis approach is described in § 4. The results are provided in § 5, followed by a summary in § 6.

Annex 1 contains material regarding background on choice of time-step value for Scatterometer 2 calculations. Annex 2 presents an example of evaluating the aggregate pulsed radio frequency interference from multiple EESS (active) spaceborne synthetic aperture radars to RNSS earth station receivers operating in the band 1 215-1 300 MHz.

2 Pulsed RFI effects

Recommendation ITU-R M.2030 provides a general method for evaluating the effect of pulsed RFI on RNSS receivers and Report ITU-R M.2220 provides a computation methodology to calculate the necessary aggregate received pulsed RFI parameters used in the evaluation. The reader is referred to these two documents for details, but a brief summary of the concepts from those documents is provided in the following sub-sections.

2.1 Effects of pulsed RFI from a single source

Pulses with a received peak power above a key RNSS receiver-dependent power level could cause varying degrees of gain compression up to full saturation in receiver analogue stages from the antenna input through the analogue-to-digital (A/D) converter. RNSS receiver saturation by strong pulses effectively reduces the amount of RNSS signal power that can be demodulated by the receiver. Weaker pulses with peak power below the key RNSS receiver-dependent level will act to effectively increase the receiver's noise floor.[1]

Strong and weak received pulse effects from a single source, *i*, are characterized in Report ITU-R M.2220 in two parameters: PDC_i and $R_{I,i}$. The unitless strong-pulse parameter, PDC_i, defined for pulse streams with peak power greater than the RNSS receiver threshold power, *Pth*, is given as:

$$PDC_i = \left(PW_{EFF,i} + \tau_r\right)PRF_i \tag{1}$$

where PRF_i is the pulse repetition frequency and τ_r is the overload recovery time of the RNSS receiver. The effective received pulse width, $PW_{EFF,i}$, is:

$$PW_{EFF,i} = PW_i\left(\frac{\Delta f}{BW_{CHIRP}}\right) \tag{2}$$

where PW_i is the transmitted pulse width of the i-th EESS sensor, BW_{CHIRP} is the sensor total linear FM chirp bandwidth, and Δf is the portion of the BW_{CHIRP} that falls within the RNSS receiver pre-correlator passband.

For the i-th EESS sensor pulse streams with peak received power, P_i, below the RNSS receiver threshold power, P_{th}, the unitless weak-pulse parameter, $R_{I,i}$, is defined as:

$$R_{I,i} = \left(\frac{1}{N_0 \cdot BW}\right)P_i \cdot dc_i \tag{3}$$

where N_0 is the RNSS receiver system input noise spectral density and *BW* is the receiver pre-correlator bandwidth. The weak-pulse duty cycle, dc_i, is given as:

$$dc_i = PW_{EFF,i} \cdot PRF_i \tag{4}$$

where $PW_{EFF,i}$ and PRF_i are defined the same as for strong pulses. Note that $R_{I,i}$ is essentially an average RFI power spectral density ratio.

2.2 Aggregate RFI cases

Given the single-source received pulse RFI parameters above, the aggregate strong and weak pulsed RFI parameters, *PDC* and R_I are defined in general for a set of *j* sources as:

$$PDC = 1 - \prod_j\left(1 - PDC_j\right) \tag{5}$$

and

$$R_I = \sum_j R_{I,j} \tag{6}$$

For the specific case of two EESS sources, equations (5) and (6) simplify to 0, 1 or 2 terms depending upon the received peak powers relative to the RNSS receiver threshold. Generally the strongest RFI impact occurs when both sources produce above-threshold received pulse streams.

Depending on which part of the EESS (active) sensor beam is illuminating an RNSS receiver, it could experience either strong or weak pulsed RFI effects from that sensor. When considering simultaneous illumination at a given time from two EESS (active) sensors, four cases are possible: strong-strong,

[1] More details of RNSS receiver pulsed effects are found in Report ITU-R M.2220, §§ 2.2.4, 2.3 and 4.1.3.

strong-weak, weak-strong and weak-weak. The analyses discussed in §§ 4 and 5 focus only on the strong-strong case when the pulsed RFI from two EESS (active) sensors both exceed the RNSS receiver's peak power threshold level. This threshold varies depending on receiver types and implementations. For these analyses this threshold level is assumed to be −129 dBW.[2]

3 EESS (active) sensors in the frequency band 1 215-1 300 MHz

3.1 General characteristics

The EESS (active) sensors in the frequency band 1 215-1 300 MHz fall in one of two categories: synthetic aperture radar (SAR) or scatterometer. The characteristics of the EESS (active) sensors used in our aggregate RFI study, SAR3, SAR6 and Scatterometer 2, are summarized in Table 1.

The EESS (active) sensors are typically deployed in sun-synchronous orbits at various altitudes. The orientation of the orbit relative to the sun is specified by the local time of the ascending node (LAN). This parameter refers to the local time of the geographical location of the satellite ground track when the EESS (active) satellite is crossing the equator in a northward path.

The EESS (active) sensors transmit pulsed waveforms, typically using linear FM modulation. The pulse widths and pulse repetition frequencies are shown in Table 1. The transmit duty cycle values range from 5.3% to 18.7%. In some cases, the sweep bandwidth of the sensor transmitter is greater than the RNSS receiver bandwidth. In such cases, the effective pulse duty cycles described in § 2.1 are used. These parameters are also listed in Table 1.

TABLE 1

EESS assumptions for SAR3, SAR6 and Scatterometer 2

Parameters	SAR3	SAR6	Scatterometer 2
Orbit assumptions			
Orbit type	Sun-synchronous	Sun-synchronous	Sun-synchronous
Orbit altitude (km)	757	628	680
Orbit inclination (degrees)	98	97.9	98
LAN	18:00	12:00 (1)	18:00
Antenna assumptions			
Antenna type	Offset-feed parabolic 15 m diameter linear array feed	Planar array 2.9 m x 9.9 m	Offset-feed parabolic 6 m diameter
Transmit antenna peak gain (dBi)	33.4	36.6	37
e.i.r.p. peak (dBW)	68.4	74.5	60
Transmit antenna elevation beamwidth (degrees)	25	4.6	2.6
Parameters	SAR3	SAR6	Scatterometer 2
Transmit antenna azimuth beamwidth (degrees)	0.8	1.3	2.6

[2] The −129 dBW threshold level is based on the Scatterometer 2 pulsed RFI effect on one particular type of RNSS receiver. See Recommendation ITU-R M.1902 for other RNSS receiver types.

TABLE 1 (*end*)

Parameters	SAR3	SAR6	Scatterometer 2
Antenna assumptions			
Transmit antenna beam look angle (degrees)	30	7.2 to 59	34
Transmit antenna beam azimuth angle (degrees)	0	7.2 to 59	0 to 360
RF assumptions			
RF centre frequency (MHz)	1 215-1 300	1 236.5, 1 257.5, 1 278.5	1 215-1 300
Polarization	Dual/quad, linear H and V	H,V, Circular and 45 degrees linear	Dual, linear H and V
Pulse modulation	Linear FM	Linear FM	Linear FM
RF bandwidth max (MHz)	78	28	1 × 2
RF pulsewidth (μs)	78	18-43	15
Pulse repetition frequency max (Hz)	2 400	1 550-3 640	3 500
Transmit ave. power (W)	598.4	428.4	10.5
e.i.r.p. average (dBW)	61.2	62.9	47.2
Transmit duty cycle (%)	18.7	6.81	10.5

(1) For SAR6, this number represents the local time of descending node.

3.2 Antenna characteristics

The azimuth and elevation antenna gain models for SAR3 and SAR6 are described in Table 2 and Table 3, respectively. The two-dimensional antenna patterns for SAR3 and SAR6 are shown in Figs 1(a) and 1(b). These SARs are side-looking radars that have antenna beams orthogonal to the sensor flight path and nadir. Depending on the SAR modes, the elevation look angles are selectable. For example, SAR6 beam can steer from 7.2 to 59 degrees in elevation.

TABLE 2

Standard SAR3 antenna gain model

Pattern	Gain $G(\theta)$ (dBi) as a function of off-axis angle θ (degrees)	Angle range
Vertical (elevation)	$G_v(\theta_v) = 35.0 - 0.18\ (\theta_v)^2$ $G_v(\theta_v) = 32.6 - 0.05\ (\lvert\theta_v\rvert - 7)^2$ $G_v(\theta_v) = 33.0 - 2.69\ (\lvert\theta_v\rvert - 12)^2$ $G_v(\theta_v) = 15.0 - 20.8 \log(\lvert\theta_v\rvert) - 0.68\ (\lvert\theta_v\rvert - 16)$ $G_v(\theta_v) = -30$	$\lvert\theta_v\rvert < 4.0°$ $4.0° \le \lvert\theta_v\rvert < 11.3°$ $11.3° \le \lvert\theta_v\rvert < 16.0°$ $16.0° \le \lvert\theta_v\rvert < 35.0°$ $\lvert\theta_v\rvert \ge 35°$
Horizontal (azimuth)	$G_h(\theta_h) = 0.0 - 15.0\ (\theta_h)^2$ $G_h(\theta_h) = -18.0$ $G_h(\theta_h) = -13.55 - 23 \log(\lvert\theta_h\rvert)$ $G_h(\theta_h) = -36.5$	$\lvert\theta_h\rvert < 1.1°$ $1.1° \le \lvert\theta_h\rvert < 1.7°$ $1.7° \le \lvert\theta_h\rvert < 10.0°$ $\lvert\theta_h\rvert \ge 10.0°$
Beam pattern	$G(\theta) = G_v(\theta_v) + G_h(\theta_h)$	

TABLE 3

Standard SAR6 antenna gain model

Pattern	Gain $G(\theta)$ (dBi) as a function of off-axis angle θ (degrees)	Angle range
Vertical (elevation)	$G_v(\theta_v) = 0.0 - 0.30\ (\theta_v)^2$ $G_v(\theta_v) = 0.0 - 0.69\ \theta_v - 7.24$ $G_v(\theta_v) = -26.0$	$0° < \lvert\theta_v\rvert < 6.20°$ $6.20° \le \lvert\theta_v\rvert < 27.00°$ $\lvert\theta_v\rvert \ge 27.00°$
Horizontal (azimuth)	$G_h(\theta_h) = 36.6 - 7.0\ (\theta_h)^2$ $G_h(\theta_h) = 36.6 - 1.43\ \theta_h - 12.83$ $G_h(\theta_h) = 36.6 - 25.0$ $G_h(\theta_h) = 36.6 - 25.0 - 34 \log(\theta_h/40)$ $G_h(\theta_h) = 36.6 - 36.98$	$0° < \lvert\theta_h\rvert < 1.46°$ $1.46° \le \lvert\theta_h\rvert < 8.47°$ $8.47° \le \lvert\theta_h\rvert < 40.0°$ $40.0° \le \lvert\theta_h\rvert < 90.0°$ $\lvert\theta_h\rvert \ge 90.0°$
Beam pattern	$G(\theta) = G_v(\theta_v) + G_h(\theta_h)$	

FIGURE 1

Antenna gain patterns for a) SAR3 and b) SAR6

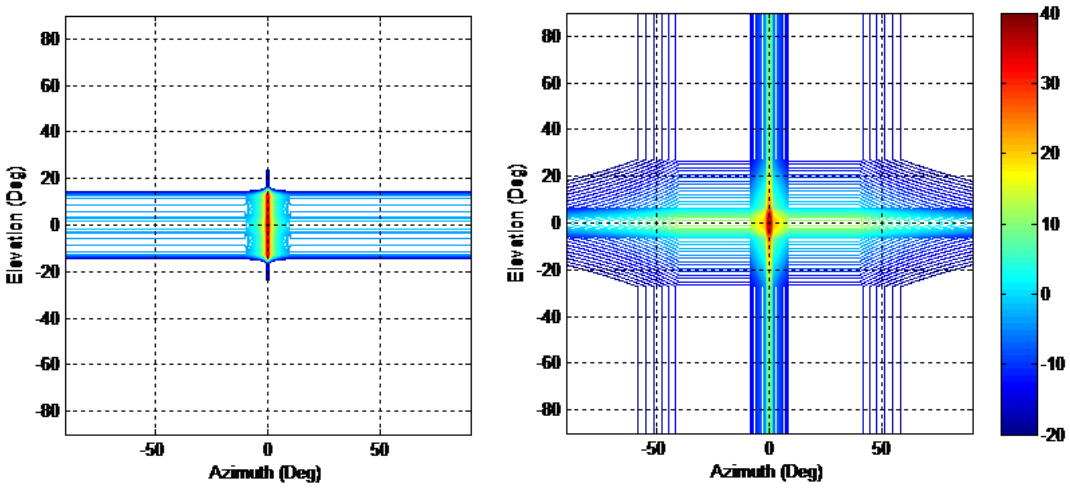

(a) (b)

The antenna gain as a function of off-axis angle for Scatterometer 2 is summarized in Table 4 while the graph of the antenna gain is shown in Fig. 2. Unlike SAR sensors with side-looking antenna beams, this scatterometer scans its antenna azimuth beam 0 to 360 degrees in azimuth at 14.6 revolutions per minute (rpm) (4.1-second rotation period).[3] As such, the antenna beam illuminates a given point on Earth for a limited period of time.

TABLE 4

Standard Scatterometer 2 antenna gain model

Pattern	Gain $G(\theta)$ (dBi) as a function of off-axis angle θ (degrees)	Angle range
Total	$G(\theta) = 36.933 - 0.0025\,(27.935\,\lvert\theta\rvert)^2$ $G(\theta) = 20.77 - 25\log(\lvert\theta\rvert)$ $G(\theta) = -21.261$	$0° < \lvert\theta\rvert < 4°$ $4 \leq \lvert\theta\rvert < 48°$ $\lvert\theta\rvert \geq 48°$

[3] The Scatterometer 2 scan rate can be set between 13.0 and 14.6 rpm (4.1 to 4.6-second rotation period). The planned revolution rate is now 13.0 rpm.

FIGURE 2

Scatterometer 2 antenna gain pattern as a function of off-axis angle

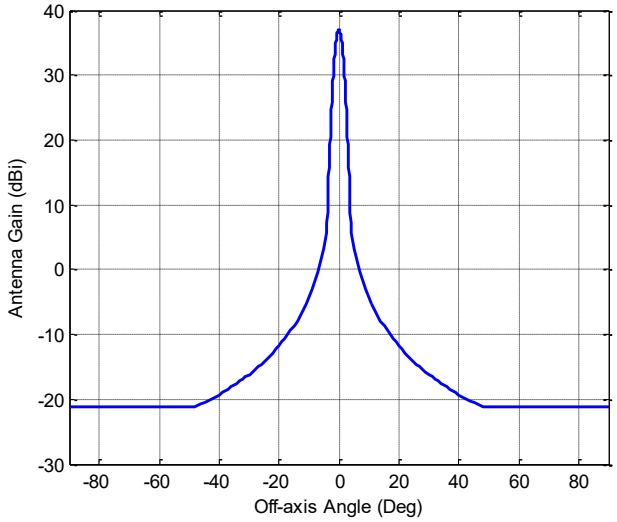

4 Aggregate RFI impingement analysis

The interference environment was simulated using the Satellite Tool Kit (STK). The first STK models of the EESS (active) satellites and the ground-based RNSS receivers were created. The STK was then used to simulate and record single-sensor received isotropic power (RIP) as seen by RNSS receivers. To build sufficient statistics, a simulation duration of 120 days was chosen.

These single-sensor RIP data sets were then post-processed in MATLAB to estimate aggregate RFI impingement statistics; i.e., how often and for how long aggregate RFI events occur. The details are described below.

4.1 Satellite models

Each EESS (active) satellite was modelled using STK's sun-synchronous orbit satellite object with the orbit parameters given in Table 1. To model the EESS (active) sensor, a transmitter component with the appropriate RF characteristics and antenna gain pattern was added to the satellite object. For SAR3 and SAR6, the antenna beam was pointed to 90 degrees in azimuth (perpendicular to the spacecraft heading) and 30 and 59 degrees in elevation, respectively. For Scatterometer 2, the antenna was assumed pointed to 34 degrees in elevation while rotating 0 to 360 degrees in azimuth at 14.6 rpm.[4]

4.2 Single sensor received isotropic power

Examples of contour plots of RIP on the Earth's surface for SAR3, SAR6 and Scatterometer 2 are shown in Figs 3(a) through (c). In each figure, the RIP contours ranging from −110 dBW to −135 dBW in 5 dB steps are displayed and the dashed circles show the coverage indicating the range to the limb of the Earth from the satellite. Any RNSS receivers in this circular area have a direct line-of-sight to the EESS (active) sensor in orbit.

Two different simulation time-steps were used, depending on the two EESS sensors under consideration. For estimating the aggregate RFI event potentials for two SARs, a 10-second time-step was used to record the RIP data. This time-step is appropriate since the SAR emission footprint moves

[4] Current plan is to use 13.0 rpm. This is the lower end of the 13.0 to 14.6 rpm range of selectable rates.

slowly across a given location on Earth and illuminates a RNSS receiver for periods lasting several minutes.

For estimating the aggregate RFI event potentials for scenarios involving Scatterometer 2, a 50-ms time-step [5] was used to properly model Scatterometer 2's rotating antenna. Since it was computationally not feasible to perform a 120-day simulation using a 50-msec time-step, a two-step approach was used. First, the STK sensor access function was used to determine times when Scatterometer 2 and a SAR were simultaneously passing over a given receiver location. For each of these times, a 10-minute simulation using 50-msec time-steps was performed to estimate the RIP data.

It should be noted that the example contours in Fig. 3 are possibly skewed with respect to actual contours due to the simplified composite EESS antenna gain formulas (Tables 2 to 4 above). If improved accuracy is needed for RNSS receiver RFI impact assessment, more complete definition may be needed in the associated EESS RS series Recommendation for active sensor antenna patterns in the sidelobe regions.

FIGURE 3

Contours of received isotropic power on the Earth's surface for SAR3, SAR6 and Scatterometer 2

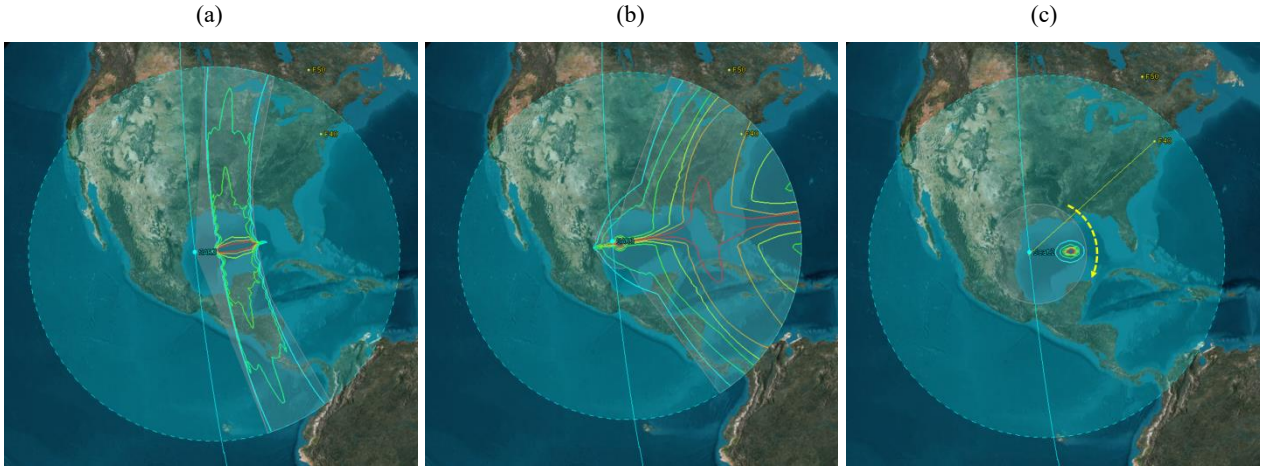

4.3 Receiver models

To determine times and durations of aggregate RFI events, victim RNSS receivers must be modelled. STK's facility object simulates placing receivers at any location on Earth. Intuitively, the simultaneous illumination events should depend on the latitudes of these receiver locations and hence RNSS receivers were placed at 40, 50, 60, 70 and 80 degrees in latitude at 75 degrees West longitude.[6]

Depending on the location of the receiver, the EESS (active) sensor appears at varying elevation angles and, consequently, the receive antenna gain was taken into consideration. The receive antenna gain pattern assumed in this analysis is shown in Fig. 4. This antenna gain pattern was taken into account during the post-processing stage of the analysis.

It should be noted that this antenna pattern represents an antenna used by one particular type of receiver. Other RNSS receivers use antennas with different gain patterns and no single gain pattern represents all RNSS receivers. Additionally, the maximum antenna gain in the lower hemisphere

---

[5] See Annex 1 for further details.

[6] The simulation also looked at 165 degrees west longitude and found that the impingement statistics changed very little.

could (under worst-case conditions) be equal to that for the upper hemisphere because the antenna in some RNSS receiver applications could potentially be pointed in almost any direction (see Table 1-1, Note 12 in Recommendation ITU-R M.1902).

FIGURE 4

Assumed RNSS receiver antenna gain as a function of elevation angle

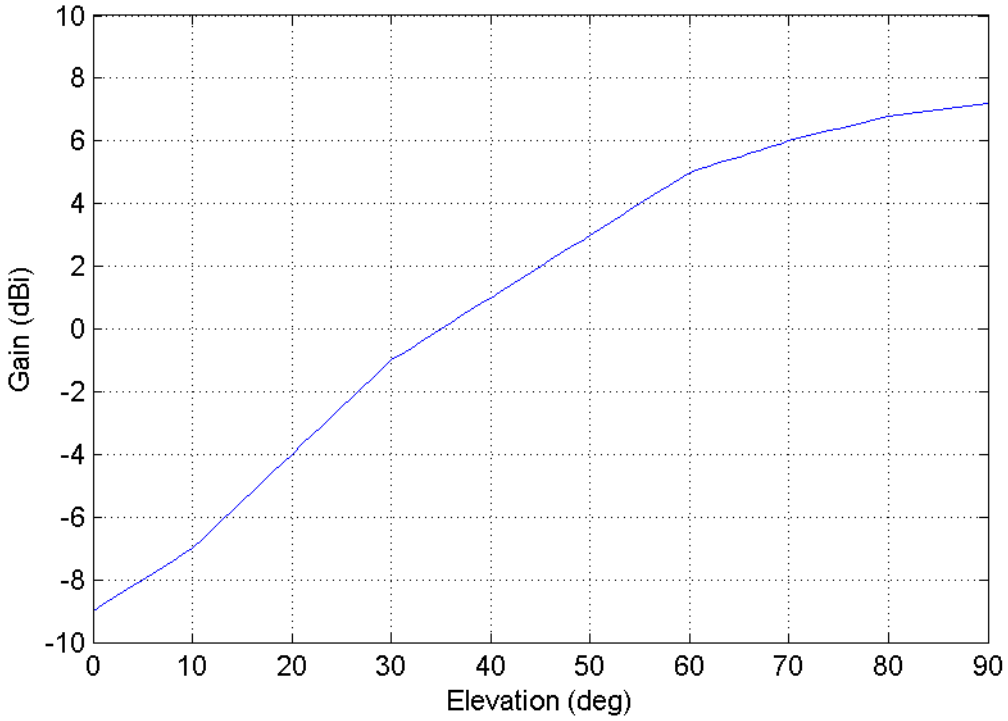

4.4 Single-sensor interference power into receivers

The single-sensor RIP datasets were post-processed to estimate the interference power into the receiver. Examples of estimated interference power, as seen by a RNSS receiver at 80 degrees latitude over a 12-hour period, are shown in Fig. 5(a) for SAR3 and SAR6. The larger emission footprint of the SAR6 wide-beam antenna impinges on receivers more frequently than SAR3. The peaks repeat about every 95 minutes, the orbital period of SAR6. Similarly, the interference power into the receiver over a single-pass, 10-minute period for Scatterometer 2 and SAR6 are shown in Fig. 6(a).

In both Figs 5(a) and 6(a), the peak power threshold level of −129 dBW is indicated by a magenta dashed horizontal line. The times when the interference power exceeds this dashed line correspond to the strong-pulse RFI case, whereas at other times they correspond to weak-pulse RFI, or no interference, cases.

The aggregate pulsed RFI cases can be better described using Fig. 7, which shows a 50-second portion of Fig. 6(a). The strong-strong pulsed RFI case is illustrated in Fig. 7 beginning at about 17:18:07 GMT (at about the 187 sec mark) when the peak pulse power from both Scatterometer 2 and SAR6 exceed the −129 dBW threshold.

For this case, equation (5) can be used to estimate the aggregate strong-pulse PDC parameter. Also shown are instances of the strong-weak pulse RFI case, immediately before and after Scatterometer 2 strong-pulse RFI occurrences. For these cases the weak-pulse parameter, RI2j, for Scatterometer 2 is non-zero and may need to be taken into account when performing pulsed RFI evaluations.

Similar strong-weak cases with Scatterometer 2 causing strong-pulse RFI and SAR6 contributing to the weak-pulse RFI are seen between 17:17:30 GMT (150 sec) and 17:18:05 GMT (185 sec). Again, the weak pulse parameter $R_{I,j}$ of SAR6 may need to be taken into account when performing pulsed RFI evaluations. The weak-weak pulse RFI case is also shown immediately before and after Scatterometer 2 strong-pulse RFI occurrences.

It is worth noting that this Report only considers the potential for simultaneous illumination events for the strong-strong pulse case. This high-level statistical analysis is simpler and more general than an analysis that would seek to quantify the RFI impact of pulsed interference to RNSS receivers and fewer RNSS receiver parameters are required. It serves to indicate whether or not aggregate pulsed RFI events could occur for the assumed set of scenarios.

4.5 Aggregate RFI impingement statistics

The aggregate RFI impingement statistics were determined by compiling records of how often and for how long the emission footprints, corresponding to the strong-strong pulse case, overlap. This was done by processing two sets of EESS data and determining the number of EESS signals exceeding the peak power threshold at any given time. The intermediate product corresponding to the data sets in Figs 5(a) and 6(a) are shown in Figs 5(b) and 6(b), respectively. In these Figures, the periods when the number of EESS signals equals 2 correspond to the strong-strong pulsed RFI case. The impingement statistics were then determined by compiling records of these peaks. These results are described in the next section.

FIGURE 5

(a) Estimated RIP for SAR3 (blue) and SAR6 (red) at 80 degrees latitude over a 12-hour period and (b) the number of strong pulsed signals seen by a receiver[7]

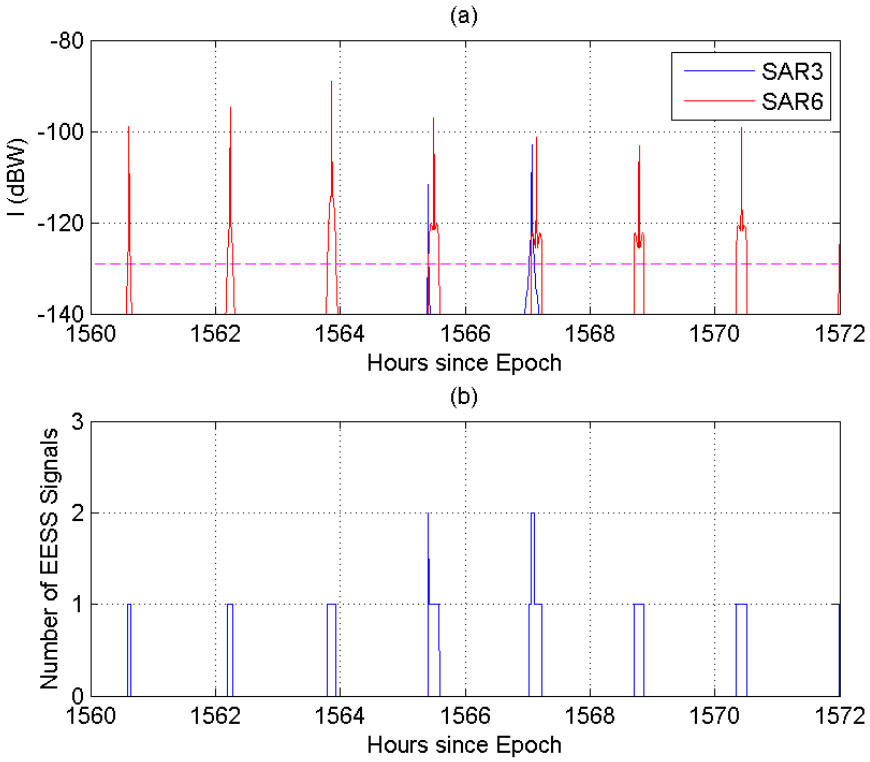

[7] For Study A, which includes current/planned missions, the planned SAR3 operational lifetime (2021-2024) does not overlap with the planned lifetimes of SAR6 (2013-2018) and Scatterometer 2 (2014-2018).

FIGURE 6

(a) Interference power into a RNSS receiver for Scatterometer 2 (blue) and SAR6 (red) at 80 degrees latitude over a ten-minute period and (b) the number of strong-pulsed signals seen by the receiver

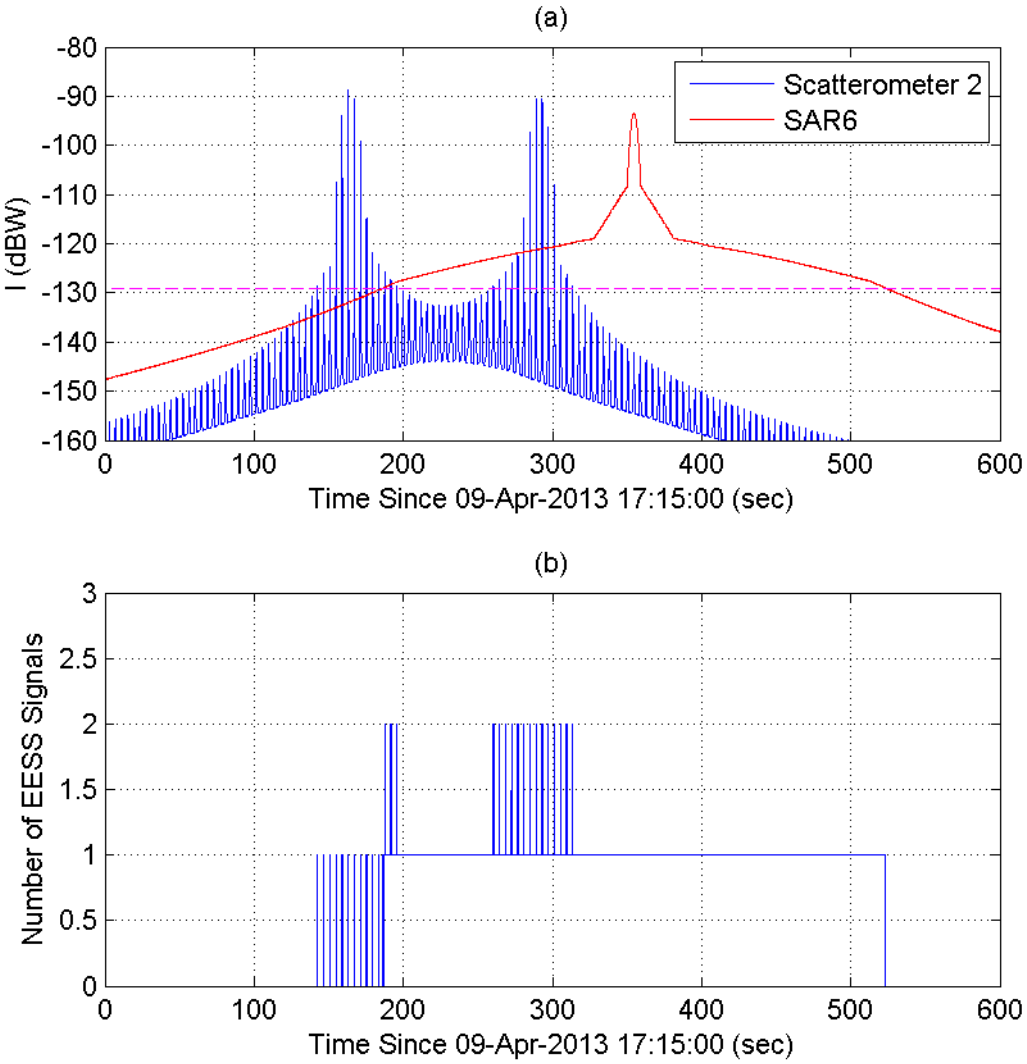

FIGURE 7

Close-up view of Fig. 6(a) showing interference power *I* (dBW)

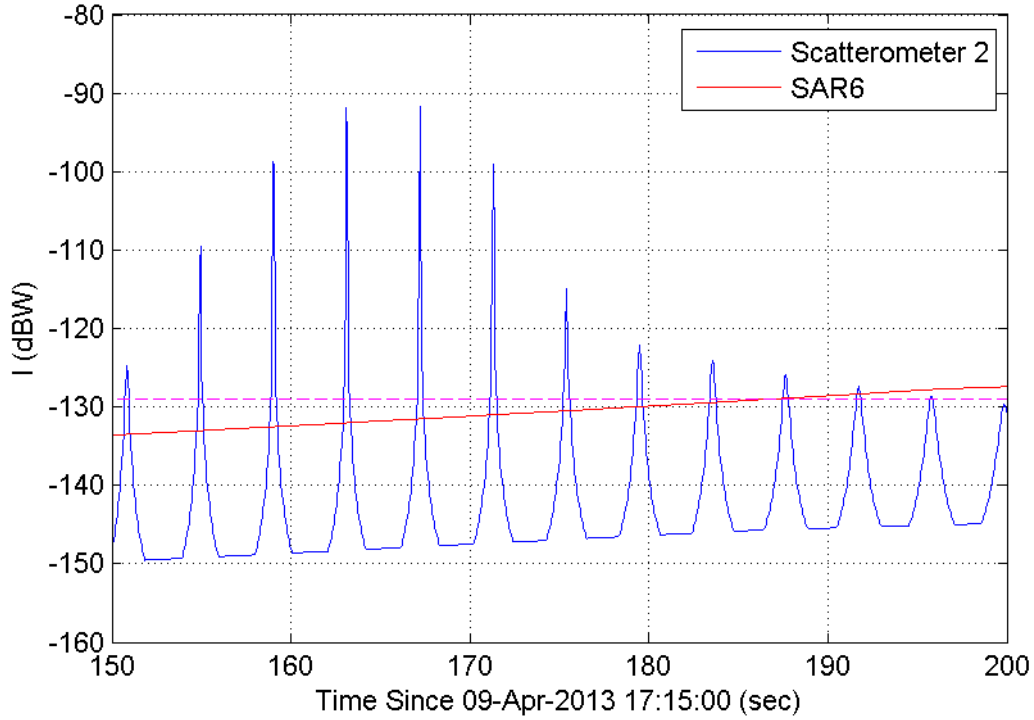

5 Analysis results

To investigate the potential for aggregate RFI, various scenarios were considered. The three Study A scenarios simulated combinations of planned EESS sensors. Study B simulated three hypothetical scenarios to explore what might happen with future deployment of EESS sensors. The description of these scenarios and results are provided in the next two sub-sections.

5.1 Study A

Study A considers planned EESS sensors and includes the following scenarios:

– SAR3 and SAR6 – a narrowbeam SAR (SAR3) and a widebeam SAR (SAR6) in orthogonal sun-synchronous orbits at different altitudes;

– SAR3 and Scatterometer 2 – a narrowbeam SAR (SAR3) and a scatterometer in the same orbit at different altitudes;

– SAR6 and Scatterometer 2 – a widebeam SAR (SAR6) and a scatterometer in orthogonal orbits at different altitudes.

The aggregate RFI impingement results for the Study A scenarios are summarized in Table 5. In all Study A scenarios, the aggregate RFI events seldom occurred during 120-day simulations. Even for the two SARs in orthogonal orbits with larger emission footprints (Scenario 1), simultaneous overlap events only occurred a total of 41 times and only at high latitude (80 degrees).

Even if the aggregate pulsed RFI for these Study A scenarios appears to be acceptable, as more EESS sensors become operational in the L2 band, the aggregate pulsed RFI will increase. This is considered in the next sub-section.

TABLE 5

Summary of Study A results over a 120-day simulation period

Scenarios		Study A		
		1 (Note 1)	2 (Note 2)	3
EESS1	LAN	18:00	18:00	12:00
	Altitude	757 km	757 km	628 km
	Antenna	Narrowbeam	Narrowbeam	Widebeam
EESS2	LAN	12:00	18:00	18:00
	Altitude	628 km	680 km	680 km
	Antenna	Widebeam	Rotating Spotbeam	Rotating Spotbeam
Comments		SAR3/SAR6 Orthogonal orbits	SAR3 Scatterometer 2 Co-planar orbits	SAR6 Scatterometer 2 Orthogonal orbits
Total Aggregate Pulsed RFI Event Occurrences (Note 3)	40 deg Lat	0	91(5)	0
	50 deg Lat	0	82(4)	0
	60 deg Lat	0	87(5)	0
	70 deg Lat	0	139(9)	6(1)
	80 deg Lat	41	409(18)	1186(63)
Duration of aggregate RFI events (max/median)	40 deg Lat	NA	0.37/0.32 (sec)	NA
	50 deg Lat	NA	0.38/0.27 (sec)	NA
	60 deg Lat	NA	0.38/0.28 (sec)	NA
	70 deg Lat	NA	0.38/0.32 (sec)	0.18/0.03 (sec)
	80 deg Lat	6.5/1.5 (min)	0.37/0.32 (sec)	0.37/0.32 (sec)

NOTE 1 – For Study A, which includes current/planned missions, the planned SAR3 operational lifetime (2021-2024) does not overlap with the planned lifetimes of SAR6 (2013-2018) and Scatterometer 2 (2014-2018).

NOTE 2 – The larger numbers of aggregate events at various latitudes do not account for the operational prohibition of simultaneously illuminating the same areas on the ground with both SAR3 and Scatterometer 2 due to concerns of mutual EESS interference.

NOTE 3 – These numbers reflect each time an individual scan of the Scatterometer antenna beam results in the received peak power envelope exceeding the strong-pulse threshold. The numbers in parenthesis for Scenarios 2 and 3 indicate the number of orbital passes when Scatterometer 2 and a SAR are simultaneously illuminating the RNSS receiver.

5.2 Study B

Study B considers the potential for aggregate RFI from possible future EESS sensors. These additional studies were considered because there could be additional EESS (active) sensors deployed in this frequency band. The following scenarios were considered:

– two widebeam SARs in orthogonal sun-synchronous orbits at different altitudes;

– two widebeam SARs in the same orbit at different altitudes;

– a visibility study for two SARs in orthogonal sun-synchronous orbits at different altitudes.

The aggregate RFI impingement results for the Study B scenarios are summarized in Table 6. Scenario 4 considers the potential for aggregate RFI should two widebeam EESS sensors be deployed

in orthogonal orbital planes. While the occurrence of beam overlap is restricted to high latitudes (> 70 degrees), the number of potential interference events is high. Scenario 5 considers the potential for aggregate RFI should two widebeam EESS sensors be deployed in the same orbit. For this particular case, the aggregate RFI events could occur at all latitudes.

Of the scenarios studied with antenna discrimination (i.e., excluding Scenario 6), Scenario 5 represents the worst configuration for two EESS sensors.[8] Finally, the visibility study for Scenario 6 indicates that, for just two EESS sensors in orthogonal orbits, the potential for significant aggregate RFI exists even at lower latitudes (> 50 degrees). Study B indicates that there is potential for harmful aggregate RFI to RNSS receivers if future EESS sensors were to be deployed with the modelled parameters.

5.3 Discussion

The analysis presented in this Report only considered the potential for two EESS (active) sensors to simultaneously illuminate an RNSS receiver. However, there are deployment plans for other EESS (active) sensors in this frequency band; for example, SAOCOM. The probability of aggregate RFI, due to three or more EESS sensors simultaneously illuminating RNSS receivers, is probably very small. However, the two-sensor EESS aggregate RFI events summarized in Tables 5 and 6 will occur more frequently.

The analysis also only considered EESS (active) sensors in 6 pm and 12 pm LAN sun-synchronous orbits. These two orbits are orthogonal to one another and provide maximum longitudinal separation. If future EESS sensors are planned for deployment in non-orthogonal orbits, the aggregate RFI impingement is likely to be worse.

For Table 5 (Study A), which considered currently planned missions, the operational duty cycle was not considered for the systems studied. Including this aspect of EESS sensor operation may reduce the number of aggregate RFI events. In addition, if there is a potential aggregate pulsed RFI occurrence, and the footprint of one or both of the SARs is illuminating the ocean, the SAR is probably not transmitting since the area of interest to operators is typically the land and coastal areas.

It is important to note that the antenna patterns used in this analysis were based on two principal plane cuts. The aggregate behaviour of antenna gain patterns and sidelobe levels of EESS systems in non-principal plane antenna patterns, therefore, may not be accurately represented by this analysis. Therefore, further studies using more accurate antenna gain patterns and orbits should be considered.

Finally, the actual quantification of aggregate RFI should be assessed based on the actual EESS sensors parameters, using the methodology in Recommendation ITU-R M.2030 and its companion Report ITU-R M.2220. Whenever such quantification indicates that a specified RNSS receiver power threshold would be exceeded during any simultaneous illumination event, then a more detailed analysis of the impact of the aggregate pulsed interference may be required to determine whether or not such aggregate pulsed interference is acceptable to the victim RNSS receiver. This important information should be taken into account for a proper investigation of potential pulsed interference mitigation techniques.

---

[8] Although the simultaneous illumination of the same point on the Earth's surface from multiple EESS sensors could potentially be avoided through operational coordination of such sensors by EESS system operators, only the mainbeam-to-mainbeam coupling is usually considered in EESS coordination. These results indicate that sidelobe illuminations should be taken into account in such coordination processes in the future.

TABLE 6

Summary of Study B results over a 120-day simulation period

Scenarios		Study B		
		4	**5 (Note 1)**	**6 (Note 2)**
EESS1	LAN	18:00	18:00	18:00
	Altitude	757 km	757 km	757 km
	Antenna	Widebeam	Widebeam	Line-of-sight
EESS2	LAN	12 PM	6 PM	12 PM
	Altitude	628 km	680 km	628 km
	Antenna	Widebeam	Widebeam	Line-of-sight
Comments		Two Widebeam EESS Orthogonal orbits	Two Widebeam EESS Co-planar orbits	Two EESS visibility study
Total Aggregate Pulsed RFI Event Occurrences	40 deg Lat	0	44	0
	50 deg Lat	0	55	25
	60 deg Lat	0	68	185
	70 deg Lat	32	116	296
	80 deg Lat	194	189	459
Duration of Aggregate RFI events (max/median)	40 deg Lat	NA	10.2/2.1 (min)	NA
	50 deg Lat	NA	10.2/2.2 (min)	6.1/3.6 (min)
	60 deg Lat	NA	10.0/2.3 (min)	11.9/5.2 (min)
	70 deg Lat	7.0/1.6 (min)	9.8/2.3 (min)	13.3/5.4 (min)
	80 deg Lat	8.2/2.3 (min)	10.3/3.3 (min)	13.4/6.6 (min)

NOTE 1 – No particular plans for widebeam SARs operating in the same orbit are known to exist at present.

NOTE 2 – In Scenario 6, for two EESS systems within line-of-sight, not all instances of the total aggregate pulsed RFI event occurrences shown may cause RFI levels above the assumed peak power threshold level of −129 dBW.

6 Summary

This Report presents results from simulations where two EESS (active) sensors are simultaneously illuminating an RNSS receiver located on the surface of the Earth. For several scenarios, the preliminary study investigated the potential for simultaneous illumination events, quantified in terms of the number and duration of instances, in which the received peak power of both of the sensors is above a specific peak power threshold (−129 dBW).

This Report identifies the potential for aggregate interference events from multiple EESS (active) sensors into RNSS receivers in terms of the number and duration of events. For a quantification of the RFI impact to an RNSS receiver, the methodology described in Report ITU-R M.2220 and Recommendation ITU-R M.2030 should be used. Such study, taking into account technical and operational characteristics of EESS (active) sensors and RNSS receivers, should be considered for future ITU-R Reports.

Annex 1

Background on choice of time-step value for Scatterometer 2 calculations

A comparison of the rapid azimuth scan rate of Scatterometer 2 in this Report (87.6°/sec) to its antenna −3 dB azimuth beamwidth (2.6°) might suggest the choice of a 50-msec time-step is too coarse to properly sample the beam motion. To address this concern, a 10-msec time-step calculation was also performed for a representative situation corresponding to that shown in Fig. 6(a). Figure 8 below shows the comparison of estimated interference power (at the output of the RNSS antenna) due to Scatterometer 2 for10-msec (blue line) and 50-msec (red dots) time steps. Note that using 50-msec time-steps will affect those antenna rotations for which the receiver is being illuminated by the peak, or very close to the peak, of the Scatterometer 2 main beam. During these scans, the interference power changes rapidly temporally because of the sharpness of the main beam. This is illustrated in Fig. 9 where the interference power estimate at the 159-second mark shows about a 3 dB difference between 10-msec and 50-msec estimates.

On the other hand, the −129 dBW interference threshold (magenta dashed line) is exceeded first during the leading edge and then later during the trailing edge of the antenna beam. For those cases, the interference power values change more slowly and under-sampling is much less likely to occur. This is illustrated in Fig. 10, which displays a close-up view between 180 to 200 seconds. In this figure, the strong pulsed event at around 196 seconds is captured using either time-step value. Thus for an initial analysis, the 50-msec time-step is believed to be adequate to sample the beam motion.

FIGURE 8

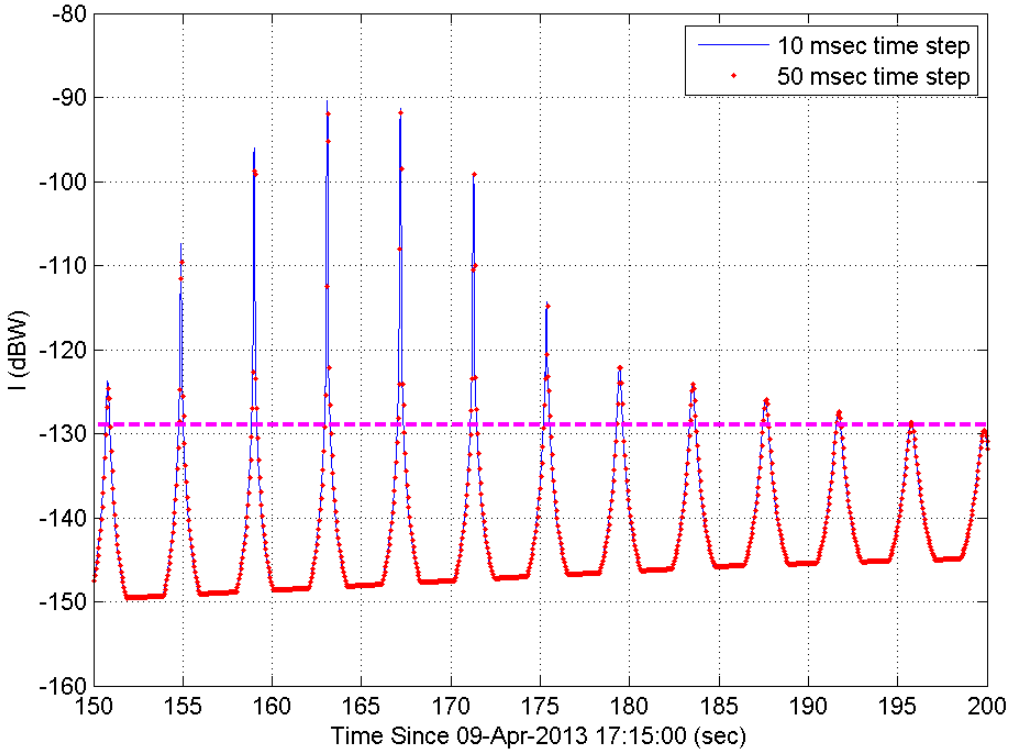

FIGURE 9

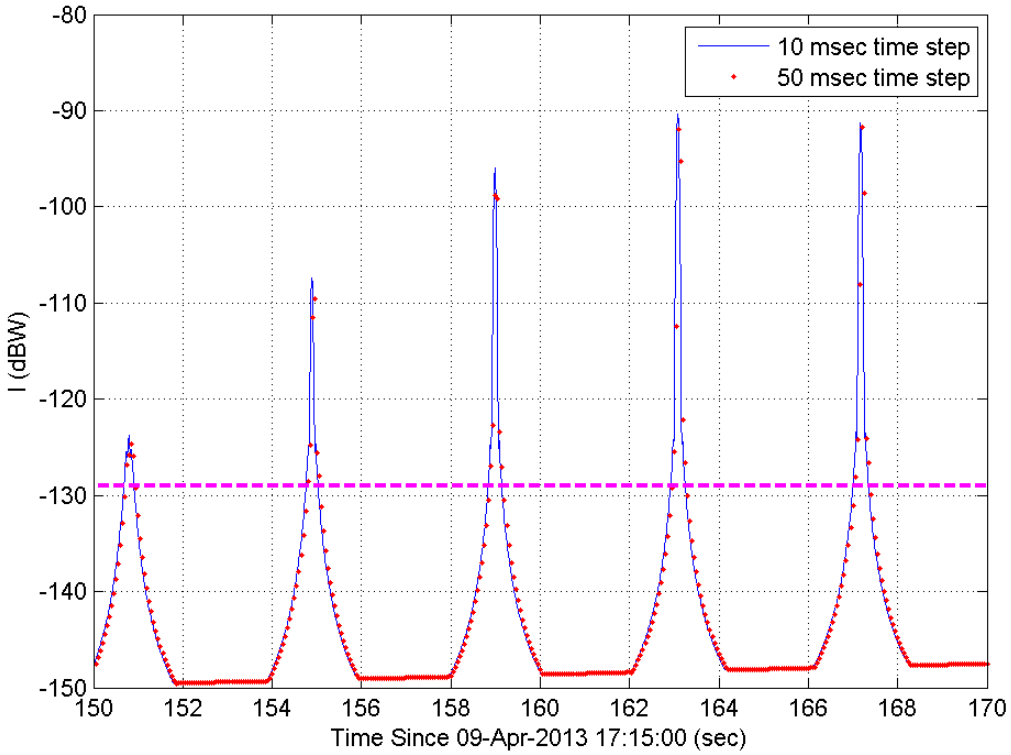

FIGURE 10

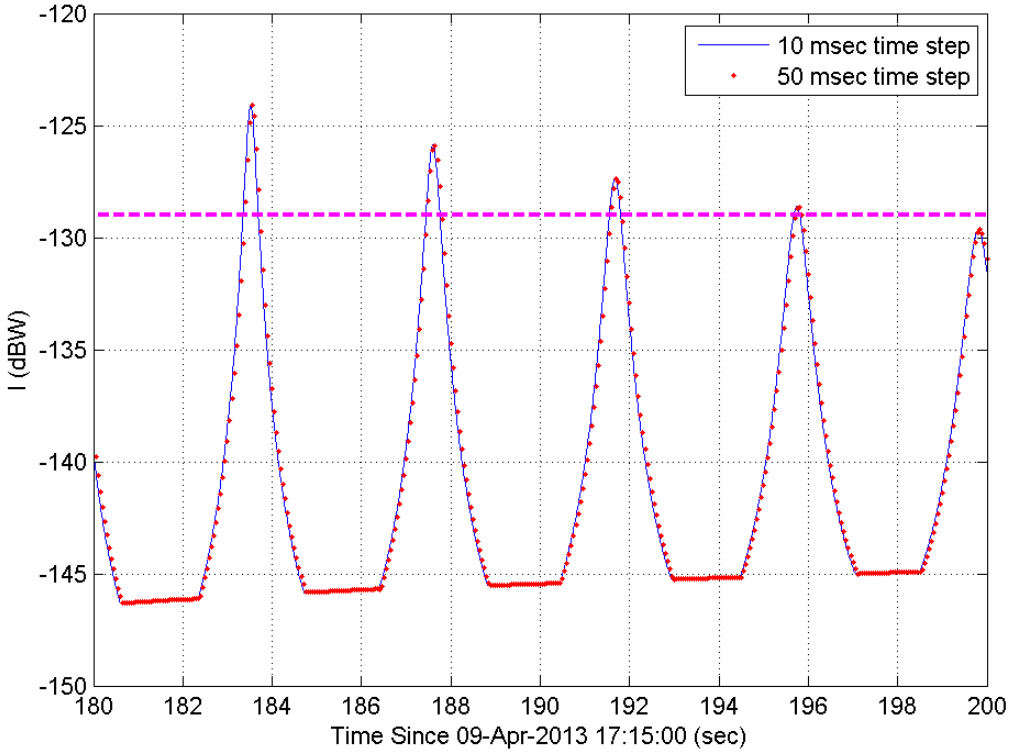

Annex 2

Example of evaluating the aggregate pulsed radio frequency interference from multiple EESS (active) spaceborne synthetic aperture radars to RNSS earth station receivers operating in the 1 215-1 300 MHz band

1 Introduction

This Annex provides an example of calculating the aggregate interference from multiple EESS (active) SAR sensors operating simultaneously over the same territory.

2 Example of evaluating the aggregate pulsed radio frequency interference from multiple spaceborne synthetic aperture radars

As an example, consider the impact of interference from the SAR1 system from Table 1 of Report ITU-R RS.2537 on an SBAS receiving RNSS earth station from column 1 to Table 7. The characteristics of SAR1 are presented in Table 7.

TABLE 7

Technical characteristics of SAR1

Parameter	Value
RF centre frequency (MHz)	1 257.5
RF bandwidth, maximum (MHz)	40
RF pulse width (μs)	33.8
Pulse repetition frequency maximum (Hz)	1 736

The effective pulsed RFI duty cycle (PDC_{LIM}) for SAR 1 is computed as follows:

$$PDC_{LIM} = (PW_{SAR1,EFF} + \tau_r)PRF_{SAR1}$$

where:

$$PW_{SAR1,EFF} = PW_{SAR1}(\frac{\Delta f}{Chirpwidth})$$

The assumed SBAS receiver recovery time (τ_r) is 1.0 μs and the SBAS receiver pre-correlator filter bandwidth is 20.5 MHz centred at 1 227.6 MHz. Considering this PDC_{LIM} for SAR1 will be:

$$PDC_{LIM,SAR1} = 0.00225$$

Using equation (8) from Annex 1 to Report ITU-R RS.2537 the degradation ratio of the pulsed interference caused by SAR1 to the SBAS receiver is the following:

$$N_{0,EFF+Y}\Big/N_{0,EFF} = \frac{1}{(1-PDC_Y)^2} \approx 1.0045$$

Or in logarithmic form $10\cdot\log_{10}(N_{0,EFF+Y}/N_{0,EFF})$ = 0.019 dB.

In accordance with Table 9 in Annex 1 of Report ITU-R RS.2537 the allowable degradation ratio of the SBAS receiver is $10\cdot\log_{10}(N_{0,EFF+Y}/N_{0,EFF})$ = 0.2 dB. Thus, the SAR1 system meets the SBAS protection criteria.

Suppose that after some time a new SAR_A system appears, which is identical in characteristics to the SAR1 system, except that the central frequency of the signal will be 1 243.85 MHz. Due to the greater overlap of frequency bands, the effective pulse duration of such a system will be longer. Applying the same equations presented above, it turns out that the value of the effective pulse duty cycle for SAR_A is:

$$PDC_{LIM,SAR_A} = 0.0223$$

Thus, the degradation ratio of the SAR_A interference impact on the SBAS receiver is $10 \cdot \log_{10}(N_{0,EFF+Y}/N_{0,EFF}) = 0.196$ dB. This system also meets the protection requirements of the SBAS receiver, since the degradation does not exceed 0.2 dB.

Now consider the cumulative impact of two systems, SAR1 and SAR_A, on the SBAS receiver in question if they operate simultaneously. Using equations (3), (4), (7) and (8) from Annex 1 to Report ITU-R RS.2537, the degradation for the SBAS receiver with simultaneous operation of SAR1 and SAR_A will be determined by the following equation:

$$N_{0,EFF+A+B} \Big/ N_{0,EFF} = \frac{1}{(1-PDC_A)^2 * (1-PDC_B)^2}$$

Or in logarithmic form:

$$10 \log_{10}\left(N_{0,EFF+A+B}/N_{0,EFF}\right) = 20 \log_{10}(1 - PDC_B)$$

Thus, the degradation of simultaneous pulsed interference impact from the two new systems is equal to the sum of the degradations of the systems while they operate separately.

$$10 \log_{10}\left(N_{0,EFF+A+B}/N_{0,EFF}\right) = 10 \log_{10}\left(N_{0,EFF+A}/N_{0,EFF}\right) + 10 \log_{10}\left(N_{0,EFF+B}/N_{0,EFF}\right)$$

Considering that for SAR1 and SAR_A systems the degradation is 0.019 dB and 0.196 dB, respectively, the total degradation will be 0.215 dB. This means that with simultaneous exposure to pulsed interference from SAR1 and SAR_A systems, the permissible degradation level for the SBAS receiver will be exceeded.

Thus, taking into account the increasing number of sources of pulsed interference, in order to correctly assess the interference effect of new pulsed systems on RNSS receivers, it is necessary to consider the current cumulative interference from all operating pulsed systems.

3 Summary

This Annex shows that when evaluating the impact of possible pulsed interference from new spaceborne synthetic aperture radars of the EESS on RNSS receivers based on the methodology of Recommendation ITU-R M.2030 as used in Report ITU-R RS.2537, it is necessary to take into account the cumulative simultaneous effect of pulsed interference from multiple sources. The methodology presented in Recommendation ITU-R M.2030 can be used for a preliminary assessment of the impact of pulsed interference to the RNSS receiver.

The issue of possible mechanisms to avoid or mitigate aggregate interference from multiple EESS (active) SAR systems requires further study, taking into account the examples in this Report.